R-7 Perturbational finite volume method for the solution of 2-D Navier-Stokes equations on unstructured colocated meshes

Z. Gao* **W. Bai***

Abstract

In this paper, perturbational finite volume (PFV) method of the Navier-Stokes equations for incompressible flow is developed. PFV scheme retains the advantages of second-order accurate central finite volume (2CFV) scheme. Both of them have the same terse formulation and use the same nodes. However, the interpolation approximation of PFV scheme is of higher order accurate. In PFV method, higher order accurate of the interpolation approximation is obtained by a numerical value pertubation technique. i.e. the mass fluxes of the cell faces are expanded into power series of the grid spacing and the coefficients of the power series are determined with the aid of the conservation equation itself. PFV schemes are used to compute the flow in a lid-driven cavity. The SIMPLE algorithm is used to predict the pressure-velocity coupling correction. Numerical results show that PFV scheme has higher accuracy, higher resolution, better stability and wider applicable range of Reynolds number than those of 2CFV scheme. For instance, in the case of coarse grid, the applicable Reynolds number ranges of second and fourth orders accurate PFV schemes are about a thousand times greater than that of 2CFV scheme.

1 INTRODUCTION.

The finite volume (FV) method has been widely used in commercial codes of computational fluid dynamics. FV method uses the integral form of the conservation equation as its starting point and can utilize conveniently diversified grids (structured and unstructured grids) and is suitable for very complex geometry, which are why it is popular with engineer. The disadvantage of the finite volume method compared to the finite difference method and finite element method is that its accuracy is not high and that FV methods of order higher than second are more difficult to develop in the three-dimensional cases[1].

The pertubational finite volume (PFV) method presented by Z. Gao[2, 3] retains the advantages of the first-order upwind and second-order central methods, however, its interpolation (or call it reconstruction) approximation are of order higher than second. In PFV method, the integral approximation is of second order accuracy, therefore, the theoretical accuracy of PFV scheme is of second-order in spite of its reconstruction approximation being of order higher than second. However, PFV schemes have some practical benefits and considerable advantages, which were verified numerically[2-4]. Numerical tests of using PFV schemes to compute the scalar transport equation show that PFV schemes have higher accuracy, higher resolution, better stability and

* Institute of Mechanics, Chinese Academy of Sciences, Beijing 100080, China

wider applicable range of Reynolds number than those of the normal second-order central scheme.

In this paper, the PFV method for the Navier-Stokes equations for incompressible fluid flow is developed, in which the SIMPLE algorithm[5, 6] is used to predict the pressure-velocity coupling correction. The flow in a lid-driven cavity is solved numerically by second and fourth-order cell-centered PFV schemes, first-order upwind and normal second-order central schemes. A comparison between numerical results of the above-cited four schemes is given and discussed.

2 PERTURBATIONAL FINITE VOLUME (PFV) SCHEME.

The general form of a scalar transport equation is

$$\frac{\partial}{\partial t}\int_V \rho\phi \mathrm{dV} + \int_S \rho\phi \mathbf{u}\cdot\mathbf{n}\mathrm{dS} = \int_S \mu\nabla\phi\cdot\mathbf{n}\mathrm{dS} \qquad (1)$$

where ϕ is the scalar variable, ρ, $\mathbf{u}$, t and μ are the fluid density, velocity, time and dynamic viscosity respectively, V and S are respectively the volume and surface area of control volume (CV), $\mathbf{n}$ is the normal unit vector of the cell face. For the case of that the line connecting two central nodes P_0 and P_j of adjacent control volumes is nearly orthogonal to the cell face, see Fig. 1 and Fig. 2, the semi-discretized cell-centered PFV schemes of second-order and fourth-order accurcy are, respectively[1, 2]

$$\frac{\partial}{\partial t}\left(V_{P_0}\phi_{P_0}\right) = \sum_{j=1}^{n_{P_0}}\left[\mu\frac{\mathbf{d}_j\cdot\mathbf{S}_j}{\left|\mathbf{d}_j\right|^2} - \frac{1}{2}F_{jf}\left(1-\frac{1}{2}R_j\right)\right]\left(\phi_{P_j}-\phi_{P_0}\right) +$$

$$\sum_{j=1}^{n_{P_0}}\left[\left(\mu\nabla\phi\cdot\mathbf{S}\right)_{jf} - \mu\frac{\mathbf{d}_j\cdot\mathbf{S}_j}{\left|\mathbf{d}_j\right|^2}\left(\phi_{P_j}-\phi_{P_0}\right)\right]^{old} \qquad (2)$$

$$\frac{\partial}{\partial t}\left(V_{P_0}\phi_{P_0}\right) = \sum_{j=1}^{n_{P_0}}\frac{1}{1+\frac{1}{6}R_j^2}\left[\mu\frac{\mathbf{d}_j\cdot\mathbf{S}_j}{\left|\mathbf{d}_j\right|^2} - \frac{1}{2}F_{jf}\left(1-\frac{1}{2}R_j+\frac{1}{6}R_j^2-\frac{1}{24}R_j^3\right)\right]\left(\phi_{P_j}-\phi_{P_0}\right) +$$

$$\sum_{j=1}^{n_{P_0}}\frac{1}{1+\frac{1}{6}R_j^2}\left[\left(\mu\nabla\phi\cdot\mathbf{S}\right)_{jf} - \mu\frac{\mathbf{d}_j\cdot\mathbf{S}_j}{\left|\mathbf{d}_j\right|^2}\left(\phi_{P_j}-\phi_{P_0}\right)\right]^{old} \qquad (3)$$

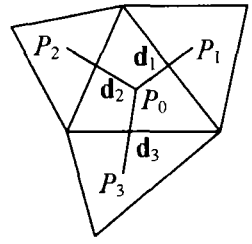

Fig. 1 Sketch of 2-D triangular meshes

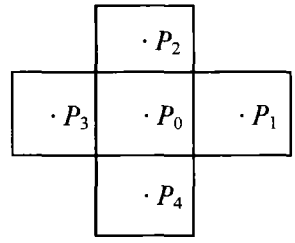

Fig. 2 Sketch of 2-D Cartesian meshes

where ϕ_{P0} is the value of ϕ at the central node P_0 of the control volume, V_{P0} is the volume of the control volume P_0, $\mathbf{d}_j$ is the vector linking two center nodes P_0 and P_j with directional being from P_0 to P_j, $\mathbf{S}_j$ is the area-vector of the j-face and its directional agrees with the outer normal of that face, $R_{jf}=F_{jf}|\mathbf{d}_j|^2/\mu\mathbf{d}_j\cdot\mathbf{S}_j$ can be considered as the cell Reynolds number in the $\mathbf{d}_j$ direction, F_{jf} is the mass flux of the cell j-face. The

continuity equation of fluid flow gives

$$\sum_{j=1}^{n_{P_0}} F_{jf} = 0 \tag{4}$$

It should be noted that both second and fourth-order accurate PFV schemes are cell centered positive FV schemes for any value of cell Reynolds number. In addition, the last terms in the right-hand side of second and fourth-order schemes (2) and (3) are usually very small, this is because that the line connecting two center nodes P_0 and P_j of adjacent control volumes is nearly orthogonal to the cell face.

3 PERTURBATIONAL FINITE VOLUME (PFV) SCHEME OF N-S EQUATIONS.

The integral form of the Navier-Stokes (NS) equations for the two-dimensional, steady, incompressible flow are

$$\int_s \rho \mathbf{u} \cdot \mathbf{n} \, \mathrm{d}s = 0 \tag{5}$$

$$\int_s \rho \mathbf{u} \phi \cdot \mathbf{n} \, \mathrm{d}s = -\int_s p \mathbf{n} \, \mathrm{d}s + \int_s \mu \, \mathrm{grad}\, \phi \cdot \mathbf{n} \, \mathrm{d}s \tag{6}$$

where $\mathbf{u}=(u, v)$, u and v are respectively the velocity components in the Cartesian x- and y-coordinate directions, p denotes the pressure.

3.1 PFV scheme of the NS momentum equation (6)

For the case of that the line connecting two center nodes P_0 and P_j of adjacent control volumes is nearly orthogonal to the cell j-face, the PFV scheme for the NS momentum equation (6) is deduced as

$$\sum_{j=1}^{n_{P_0}} \frac{1}{1+\frac{1}{6}R_j^2} \left[\mu \frac{\mathbf{d}_j \cdot \mathbf{S}_j}{|\mathbf{d}_j|^2} - \frac{1}{2} F_j \left(1 - \frac{1}{2} R_j + \frac{1}{6} R_j^2 - \frac{1}{24} R_j^3 \right) \right]$$

$$\left(\phi_{P_j} - \phi_{P_0} \right) - \sum_{j=1}^{n_{P_0}} p_j \mathbf{S}_j +$$

$$\sum_{j=1}^{n_{P_0}} \frac{1}{1+\frac{1}{6}R_j^2} \left[(\mu \nabla \phi \cdot \mathbf{S})_j - \mu \frac{\mathbf{d}_j \cdot \mathbf{S}_j}{|\mathbf{d}_j|^2} \left(\phi_{P_j} - \phi_{P_0} \right) \right]^{old} = 0 \tag{7}$$

in which the term, labeled *old*, is computed in the previous iteration. Above equation is finally expressed as

$$a_0 \phi_{P_0} = \sum_{j=1}^{n_{P_0}} a_j \phi_{P_j} + b_0 \tag{8}$$

where

$$a_j = \frac{1}{1+\frac{1}{6}R_j^2} \left[\mu \frac{\mathbf{d}_j \cdot \mathbf{S}_j}{|\mathbf{d}_j|^2} - \frac{1}{2} F_j \left(1 - \frac{1}{2} R_j + \frac{1}{6} R_j^2 - \frac{1}{24} R_j^3 \right) \right] \tag{9}$$

$$a_0 = \sum_{j=1}^{n_{P_0}} a_j \tag{10}$$

$$b_0 = -\sum_{j=1}^{n_{P_0}} p_j \mathbf{S}_j + \sum_{j=1}^{n_{P_0}} \frac{1}{1+\frac{1}{6}R_j^2} \left[(\mu \nabla \phi \cdot \mathbf{S})_j - \mu \frac{\mathbf{d}_j \cdot \mathbf{S}_j}{|\mathbf{d}_j|^2} \left(\phi_{P_j} - \phi_{P_0} \right) \right]^{old} \tag{11}$$

The under-relaxation is always used in the numerical computation to avoid the divergence of the iterative procedure[7]. Therefor we use the following equation instead of the discretized momentum equation (8)

$$\left(\frac{a_0}{\alpha_\phi}\right)\phi_{P_0} = \sum_{j=1}^{n_{P_0}} a_j \phi_{P_j} + b_0 +$$

$$\left(1-\alpha_\phi\right)\frac{a_0}{\alpha_\phi}\phi_{P_0}^{old} \qquad (12)$$

where α_ϕ is the under-relaxation factor for the variable ϕ, and it is equal to 0.7 in present paper.

3.2 The pressure-velocity coupling correction equation and its numerical discretization

Regarded the pressure p^*_{P0} determined in the previous iteration as the initial value of the present iteration, the initial velocity $\mathbf{u}^*_{P0}$ can be obtained by solving the discretized momentum equation (12), which is not necessary to satisfy the continuity equation. Therefor the SIMPLE algorithm is adopted here to obtain the corrections for the initial pressure and velocity, in which the correction for the cell face velocity $\mathbf{u}'_j$ is defined as:

$$\mathbf{u}'_j = -\frac{1}{2}\left[\left(\frac{V}{a_0}\right)_{P_0} + \left(\frac{V}{a_0}\right)_{P_j}\right] + \left(\frac{p'_{P_j} - p'_{P_0}}{|\mathbf{d}_j|}\right)\frac{\mathbf{S}_j}{|\mathbf{S}_j|} \qquad (13)$$

where p'_{P0} and p'_P are the pressure corrections of the control volume (CV) P_0 and P_j respectively. The linear interpolation of the initial velocity $\mathbf{u}^*_{P0}$ is adopted to obtain the cell face velocity $\mathbf{u}^*_j$. Then $\mathbf{u}_j'$ should make $(\mathbf{u}^*_j + \mathbf{u}_j')$ satisfy the continuity equation. Substituting above equation into the continuity equation, we can reach the following discretized equation about the pressure correction p'_{P0}

$$a_0^p p'_{P_0} = \sum_{j=1}^{n_{P_0}} a_j^p p'_{P_j} + b_0^p \qquad (14)$$

where the superscript p denotes that the coefficients are in the pressure-correction equation. And the coefficients are given by

$$a_j^p = \frac{1}{2}\left[\left(\frac{V}{a_0}\right)_{P_0} + \left(\frac{V}{a_0}\right)_{P_j}\right]\frac{|\mathbf{S}_j|}{|\mathbf{d}_j|} \qquad (15)$$

$$a_0^p = \sum_{j=1}^{n_{P_0}} a_j^p \qquad (16)$$

$$b_0^p = -\sum_{j=1}^{n_{P_0}} F_j \qquad (17)$$

where $b_0{}^p$ denotes the sum of mass fluxes through the faces of the CV P_0. After obtained the pressure correction p'_{P0}, the pressure and the velocity are corrected by

$$p_{P_0} = p^*_{P_0} + \alpha_p p'_{P_0} \qquad (18)$$

$$\mathbf{u}_{P_0} = \mathbf{u}^*_{P_0} - \frac{V_{P_0}}{a_0^u}\nabla p'_{P_0} = \mathbf{u}^*_{P_0} - \sum_{j=1}^{n_{P_0}} \frac{p'_j \mathbf{S}_j}{a_0^u} \qquad (19)$$

where α_p is the under-relaxation factor for the pressure, which is given 0.5 here.

4 NUMERICAL TESTS FOR THE FLOW IN A LID-DRIVEN CAVITY.

Some numerical results of using the present cell-centered PFV scheme, second-order central and first-order upwind schemes to compute the viscous flow in a lid-driven cavity are given and compared with those of the benchmark solution[8]. 2158 triangular elements generated by the Delaunay triangulation method are adopted, as shown in Figure 3. The algebraic equation system is solved by the Gauss-Seidel method. The estimated convergence error of the inner iteration is the maximum relative error between two neighboring iterations, the convergence criterion is 1×10^{-6}. The estimated convergence error of the outer iteration is the global mass flux residue, and the convergence criterion is 1×10^{-5}.

Fig. 4 and Fig. 5 give the horizontal and vertical velocity components u and v at the vertical and horizontal centerlines of the cavity, respectively. The computational results of PFV

schemes match the benchmark solution well. In the benchmark solution[8], the multigrid technique was used and the mesh-number reaches to 320×320, which is about 47times greater than that adopted in PFV solution.

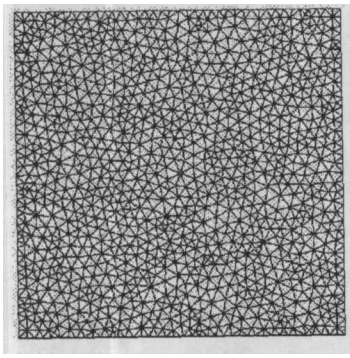

Fig.3 Triangular meshes for the flow in a lid-driven cavity

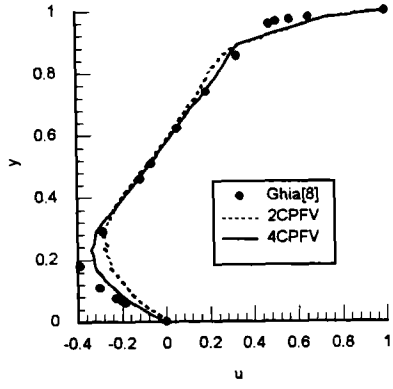

Fig. 4 Horizontal velocity component u at the vertical centerline

For the case of Reynolds number being equal to 10^4, Fig. 6 gives an estimation of convergence of the global mass flux residue. The convergence rates of the second and fourth-order cell-centered PFV schemes are respectively about 7 and 5 times as fast as the first-order upwind scheme. Moreover, both solutions of second and fourth-order PFV schemes converge monotonously with increase of iterative numbers, the solution of first-order upwind scheme is not monotonously convergence.

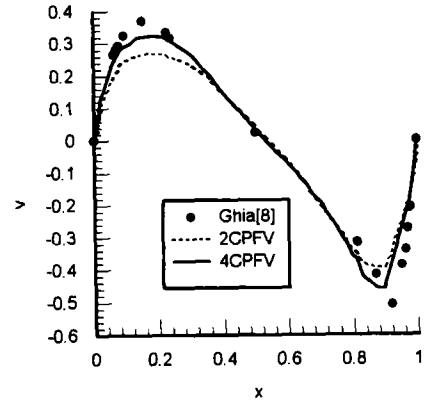

Fig. 5 vertical velocity component v at the horizontal centerline

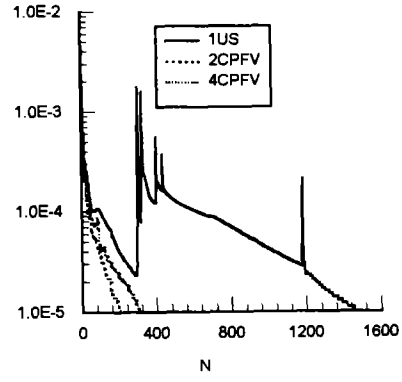

Fig. 6 Global mass flux residue (N: Numbers of iterations)

Tab. 1 gives a comparison of applicable Reynolds number ranges of the PFV schemes with that of second-order central scheme(2CS). In the case of coarse grid the applicable Reynolds number ranges of second and fourth-order PFV schemes are about a thousand times greater than that of the normal second-order scheme. The applicable Reynolds number ranges are expanded so much, this is because of that both second and fourth-order PFV schemes are positive one for any value of grid Reynolds number and that the normal second-order central scheme is positive one only when the grid Reynolds number is less than two. The meshes will become not well-distributed with locally crowded of meshes, which will weaken the advantages of PFV

Table. 1 Applicable Reynolds number ranges of PFV and normal second-order central schemes.

Number of control volume: N	Equivalent grid number in the x direction: $(N/2)^{1/2}$	2CS		2CPFV		4CPFV	
		$maxR_e$	$maxR_\Delta$	$maxR_e$	$maxR_\Delta$	$maxR_e$	$maxR_\Delta$
200	10	114	11.4	1.13×10^5	1.13×10^4	6.82×10^5	6.82×10^4
1.8×10^3	30	360	12.0	2.75×10^5	9.2×10^3	2.78×10^5	9.3×10^3
3.2×10^3	40	368	9.2	4.44×10^5	1.1×10^4	4.41×10^5	1.1×10^4
5.0×10^3	50	378	7.56	1.37×10^3	2.7×10^1	1.31×10^3	2.6×10^1
7.2×10^3	60	562	9.37	1.89×10^3	3.2×10^1	1.66×10^3	2.8×10^1
1.28×10^4	80	477	5.96	3.52×10^3	4.4×10^1	2.59×10^3	3.2×10^1

schemes, however, the applicable Reynolds number ranges of PFV schemes have increased by three to eight times compared with that of the second-order central scheme(2CS).

5 CONCLUSION.

Perturbational finite volume (PFV) scheme of the Navier-Stokes equations for incompressible flow has the same terse formulations and uses the same nodes as those of the normal second-order central scheme. However, the reconstruction approximations of PFV schemes are of higher order accuracy, PFV scheme has some practical benefits and considerable advantages. Numerical results of using PFV schemes, first-order upwind, and second-order central scheme to compute the flow in a lid-driven cavity show that PFV scheme's accuracy, resolution, efficiency and applicable Reynolds number range are higher (or larger) than those of the normal second-order central scheme.

ACKNOWLEGEMENT This work was sponsored by the National Natural Science Foundation of China (Contract No.10272106, 10032050)

REFERENCES

1 Ferziger J H, Peric M. Computational methods for fluid dynamics (2nd edit). Springer, 1999.

2 Z. Gao. Perturbational finite volume method for convective-diffusion equation and discussion (in Chinese). In Proc. 11th National Conference on Computational Fluid Dynamics(pp.29-35), Luoyang, China, Sep., 2002(To be published in Acta Mechanics Sinica.)

3 Gao Zhi. Perturbational finite volume method — a numerical-value perturbation treatment of solving convective diffusion integral equation. ICM2002-Beijing, Satellite Conference on Scientific Computing, Aug. 2002,Xi'an (pp30-31).

4 Z. Gao, H. Xiang. Perturbational finite volume method and the significance of higher order accuracy of reconstruction approximation (in Chinese). In Proc. 4th Cross-Strait CFD Workshop, Yunnan, China, April, 2003.

5 Patankar S V, Spalding D B. A calculation procedure for heat, mass and momentum transfer in three-dimensional parabolic flows. Int. Jour. Heat Mass Transfer, 1972, 15, 1787-1806.

6 Van Doormaal J P, Raithby G D. Enhancement of the SIMPLE method for predicting incompressible fluid flows. Numer. Heat Transfer, 1984, 7, 147-163.

7 Peric M. Analysis of pressure velocity coupling on nonorthogonal grids. Numer. Heat Transfer, Part B, 1990, 17, 63-82.

8 Ghia, U, Ghia, K N, Shin, C T. High Re-solutions for incompressible flow using the Navier-Stokes equations and a multigrid method. Jour. Comp. Phys., 1982, 48, 387-411.